



Electrorefining of nickel from nickel–chromium alloy in molten LiCl–KCl

Tie-Jian Zhu¹ · Wei Huang¹ · Qing-Nuan Li¹

Received: 28 December 2018 / Revised: 8 April 2019 / Accepted: 5 May 2019 / Published online: 12 August 2019

© China Science Publishing & Media Ltd. (Science Press), Shanghai Institute of Applied Physics, the Chinese Academy of Sciences, Chinese Nuclear Society and Springer Nature Singapore Pte Ltd. 2019

Abstract Electrorefining of nickel in LiCl–KCl melt was investigated using electrochemical techniques. Nickel products after electrorefining were characterized by X-ray diffraction, X-ray fluorescence, and scanning electron microscopy. Both cyclic voltammetry and square wave voltammetry results suggested that Ni^{2+} was directly reduced to Ni metal in LiCl–KCl. Based on a preliminary study on the electrochemical behavior of nickel and chromium, electrorefining was carried out under constant potential, whereupon deposits were formed on the cathode. The purity of nickel increased from 72.62% in the original alloy to 99.83% in cathodic deposits, as determined by inductively coupled plasma atomic emission spectroscopy analysis. Almost all the nickel in the alloy could be recovered during the electrochemical process with > 90% current efficiency. A lower concentration of NiCl_2 in LiCl–KCl was found to be favorable for nickel electrorefining, as increased NiCl_2 concentration caused severe corrosion of the nickel anode at the gas–liquid interface due to the accumulation of Cl_2 gas.

Keywords Electrorefining · Nickel · Molten salt · Alloy · LiCl–KCl

This work was supported by the National Nature Science Foundation of China (Nos. 21601200 and 21771188), Strategic Priority Research Program and Frontier Science Key Program (Nos. XD02030000 and QYZDY-SSW-JSC016) of the Chinese Academy of Sciences.

✉ Tie-Jian Zhu
zhtiejian@sinap.ac.cn

¹ Department of Radiochemistry, Shanghai Institute of Applied Physics, Chinese Academy of Sciences, Shanghai 201800, China

1 Introduction

Nickel is widely used in modern industry due to its high catalytic activity [1, 2] and high corrosion resistance [3, 4]. High-purity metallic nickel has been obtained using a variety of processes, including the sublimation of nickel carbonyl [5, 6], electrorefining [7], and distillation [8], among which electrorefining is a promising option widely used in metallurgy [9–11]. However, experimental studies on nickel electrorefining reported so far have been performed in weakly acidic solutions containing NiCl_2 or NiSO_4 . Although impurities, such as Co, Fe, Cu, and S, present in crude nickel can be removed by electrorefining, the concomitant evolution of H_2 at the cathode occurs due to the acidic nature of the electrolyte, which competes with nickel deposition [12, 13]. Such side reactions dramatically reduce the current efficiency and also cause the formation of unwanted products like $\text{Ni}(\text{OH})_2$ gel as the pH of electrolyte is increased, eventually hampering the growth of metallic nickel on the cathode.

As an alternative to nickel electrorefining in aqueous solution, high-temperature molten salt media have been successfully used in electrometallurgy and electrowinning due to their unique characteristics [14, 15]. The high diffusion rate of ions as well as the high conductance of molten salt can improve current efficiency and promote the deposition of products on the electrode during electrorefining [16, 17]. A series of studies have been performed on electrorefining of different metals and nonmetals in molten chlorides, including zirconium [18], magnesium [19], uranium [20], aluminum [21], and silicon [22].

To the best of our knowledge, electrorefining of nickel in molten chloride has not been investigated so far. In this paper, we report experimental results on the electrorefining

of nickel from a nickel–chromium alloy in LiCl–KCl molten salt at constant potential. The composition and morphology of the deposits formed on the cathode were characterized by X-ray diffraction (XRD), X-ray fluorometry (XRF), and scanning electron microscopy (SEM). The purity of the deposit was determined by inductively coupled plasma atomic emission spectroscopy (ICP-AES). The influence of nickel concentration in the molten chloride on current efficiency is also discussed.

2 Experimental section

2.1 Materials

LiCl, KCl (99%), and NiCl₂ (99.9%) (Sigma-Aldrich) were used without further purification; the nickel–chromium alloy (Menghe resistor factory, Changzhou, China) contained 72.62 wt% nickel and 21.84 wt% chromium. Other impurities (5.54 wt%) included Si, Sb, Mn, Al, Fe, Ti, and Mo. The LiCl–KCl eutectic salt was prepared according to previously reported procedures [23, 24], and the NiCl₂–LiCl–KCl melt was obtained by mixing LiCl–KCl eutectic and NiCl₂ followed by heating at 723 K for 2 h.

2.2 Electrochemistry

Electrochemical experiments were carried out using a setup described in detail in a previous report [25, 26]. Briefly, the measurement setup consisted of an argon glove box, an electric resistance furnace with a stainless steel vessel, and an off gas treatment unit. The concentrations of O₂ and H₂O were maintained at < 1 ppm inside the argon glove box. LiCl–KCl–NiCl₂ mixtures were loaded into an alumina crucible placed in the stainless steel vessel, which was heated to 723 K using a furnace that precisely maintained this temperature with variations less than ~ 1 K. All the electrochemical experiments were carried out at 723 K.

A three-electrode system was used for the electrochemical investigations. The working electrode for cyclic voltammetry (CV) and square wave voltammetry (SWV) measurements was a tungsten wire (99.9%, Φ1, Alfa-Aesar), cleaned by ultrasonic treatment in diluted HNO₃ (1.6 mol/dm³) and dried overnight under vacuum. Electrorefining was carried out under constant potential while simultaneously tracing the chronoamperogram. To improve deposition efficiency, a stainless steel screw (M6, active electrode area 7.22 cm²) was used as the working electrode during electrorefining. A standard Ag/AgCl (5 mol% AgCl in LiCl–KCl) electrode served as the reference electrode, and a graphite rod (Φ3) was used as the auxiliary electrode

in all the experiments. All the electrochemical experiments were performed on an Autolab PGSTAT N302 (Metrohm) electrochemical workstation controlled by NOVA (1.10 version) software. Transient techniques, such as CV and SWV, were used to examine the electrochemical behavior of Ni²⁺/Ni⁰ in LiCl–KCl molten salt.

2.3 Sample analysis

The obtained metal deposits were dissolved in nitric acid, and the concentration of nickel was determined in the solutions by ICP-AES (Optima 8000, PerkinElmer). XRD (X'PERT POWDER, PANalytical, copper K_α source) and XRF were performed to characterize the deposited products. The morphology of the deposits was studied by SEM (Phenom ProX).

3 Results and discussion

3.1 Electrochemical behavior of Ni²⁺ in LiCl–KCl molten salt

There are two main steps in the electrorefining of a crude material in a molten salt: the dissolution of the anodic crude material under a certain positive current and the deposition of dissolved metal ion on the cathode. Impurities with oxidation potentials ($E_{\text{diss}}^{\text{impurity}}$) more positive than that of nickel ($E_{\text{diss}}^{\text{Ni}}$) remain on the anode. If $E_{\text{diss}}^{\text{impurity}}$ is more negative than $E_{\text{diss}}^{\text{Ni}}$, dissolved impurities will remain in the electrolyte and high-purity nickel can be deposited on the cathode [27, 28]. Although the electrochemical behavior of chromium (major impurity in the alloy) in molten chloride has been reported [29], there is little information on the electrochemistry of nickel in this system. Therefore, we first investigated the electrochemical behavior of Ni²⁺ in LiCl–KCl to determine both the reduction potential of nickel and the number of electrons exchanged in the reduction process.

Figure 1 shows the cyclic voltammogram of molten LiCl–KCl containing 0.58 wt% NiCl₂ at 723 K. A clear negative current peak at – 0.20 V is seen with the corresponding positive current peak appearing at 0.0 V. Since no peak is observed in the cyclic voltammogram of pure LiCl–KCl (used as a blank) in the voltage range of – 1.2 to 0.4 V, we infer that both the peaks should arise from the redox reactions of nickel in LiCl–KCl. A series of cyclic voltammograms were obtained by varying the scan rate from 0.05 to 0.25 V/s. As shown in Fig. 2a, the cathodic peak slightly shifts in the negative direction with increasing scan rate. The mid-peak potential (E_{mp} , defined as half of the sum of cathodic and anodic peak potentials) remains nearly independent of the scan rate as shown in Fig. 2b,

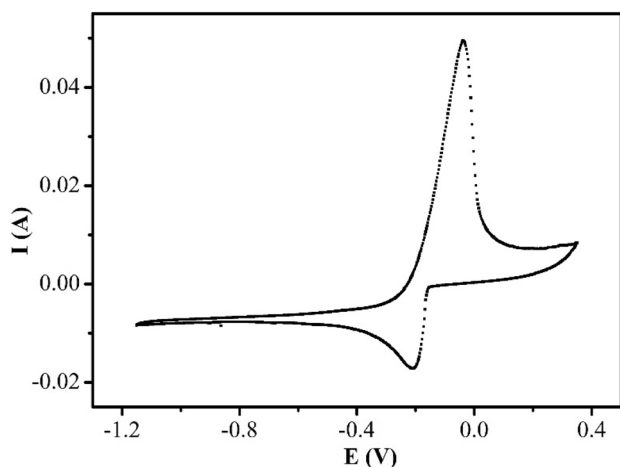


Fig. 1 Cyclic voltammogram of LiCl–KCl–NiCl₂ (0.58 wt%) at the scanning rate of 0.1 V/s at 723 K. Working electrode: tungsten wire ($S = 0.32 \text{ cm}^2$); reference electrode: Ag/AgCl; auxiliary electrode: graphite rod ($\Phi 3$)

which further confirms that the electrochemical process is reversible [30]. For a simple reversible reaction, the half-wave width, $W_{1/2}$, obtained in a square wave voltammogram depends on the number of electrons exchanged and the temperature, as given by Eq. 1 [31]:

$$W_{1/2} = 3.52RT/nF, \quad (1)$$

where R is the ideal gas constant (8.314), T is the temperature in K, n is the number of electrons exchanged during the electrochemical reaction on the electrode, and

F is the Faraday constant (96,485). From Eq. 1 and obtaining $W_{1/2}$ from Fig. 2c, the number of electrons exchanged is calculated to be 1.8, suggesting that Ni^{2+} is directly reduced to metallic Ni in LiCl–KCl by a two-electron process and the redox peaks at -0.2 and 0.0 V arise from the redox couple Ni^{2+}/Ni .

3.2 Electrorefining of nickel from nickel–chromium alloy

Cotarta et al. [29] have studied the electrochemistry of chromium in LiCl–KCl molten salt and measured the redox potential of chromium. Cr(III) can be reduced to Cr metal stepwise through two electrochemical reactions mediated by Cr(II) at 0.1 and -0.9 V (vs. Ag/AgCl). Based on the electrochemical behavior of nickel and chromium, it is noted that both metals can be electrochemically dissolved in LiCl–KCl melt as Ni^{2+} and Cr^{3+} ions at 0 and 0.2 V. According to the CV results in Fig. 1, the reduction potential of Ni^{2+} is located at -0.2 V (vs. Ag/AgCl); the redox reactions involved in the complete process are listed as follows:

Anodic reaction:

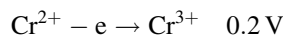
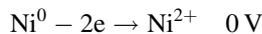
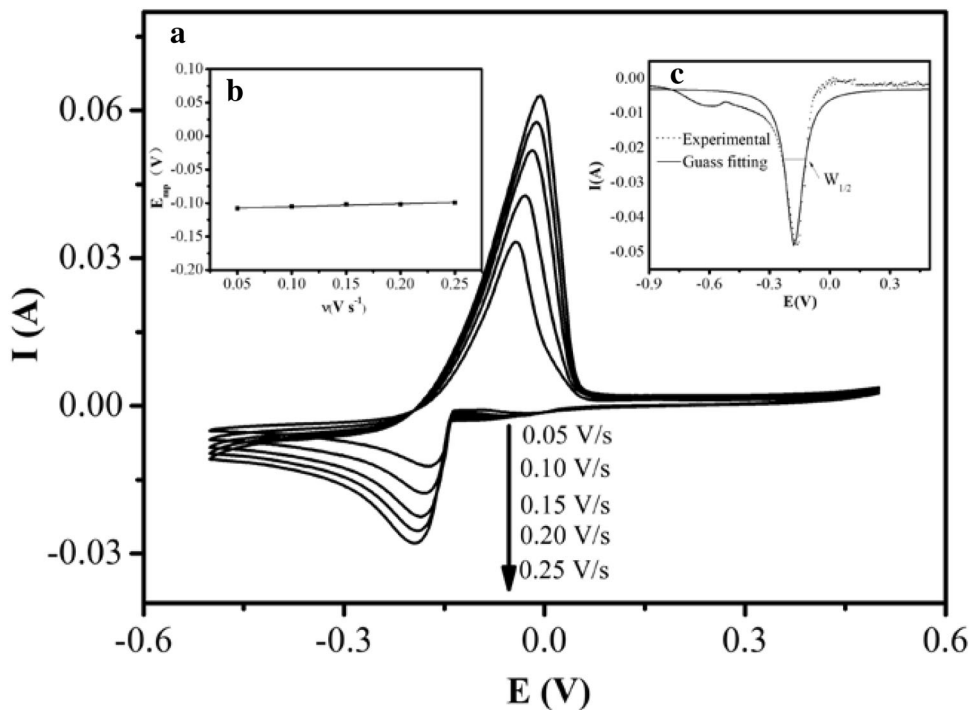
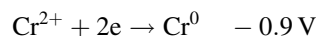
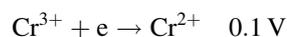
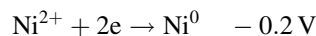


Fig. 2 a Cyclic voltammograms of LiCl–KCl–NiCl₂ (0.58 wt%) at different scanning rates, **b** plot of the relation between mid-peak potential and scanning rate, **c** square wave voltammogram with a frequency of 20 Hz; working electrode: tungsten wire, ($S = 0.32 \text{ cm}^2$), reference electrode: Ag/AgCl; auxiliary electrode: graphite rod ($\Phi 3$)



Cathodic reaction:



It is seen from the above equations that the difference between the deposition potentials of Ni^{2+} and Cr^{2+} is 0.7 V. According to reports by Li et al. [32–34], the theoretical potential difference between the apparent standard potentials of nickel and chromium depends on the recovery rate η , the number of exchanged electrons, and the initial concentration of the two metal ions. Supposing $\eta_{\text{Ni}} = 99.999\%$ and $\eta_{\text{Cr}} = 0.01\%$, a difference $> 0.36 \text{ V}$ in the deposition potentials of nickel and chromium is sufficient to achieve selective deposition at 723 K. Therefore, it is

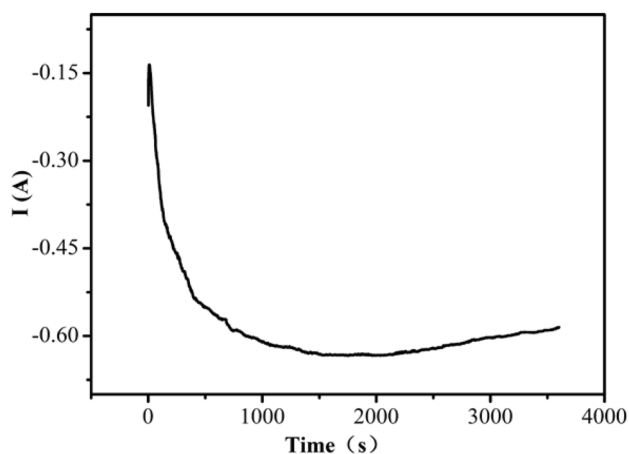


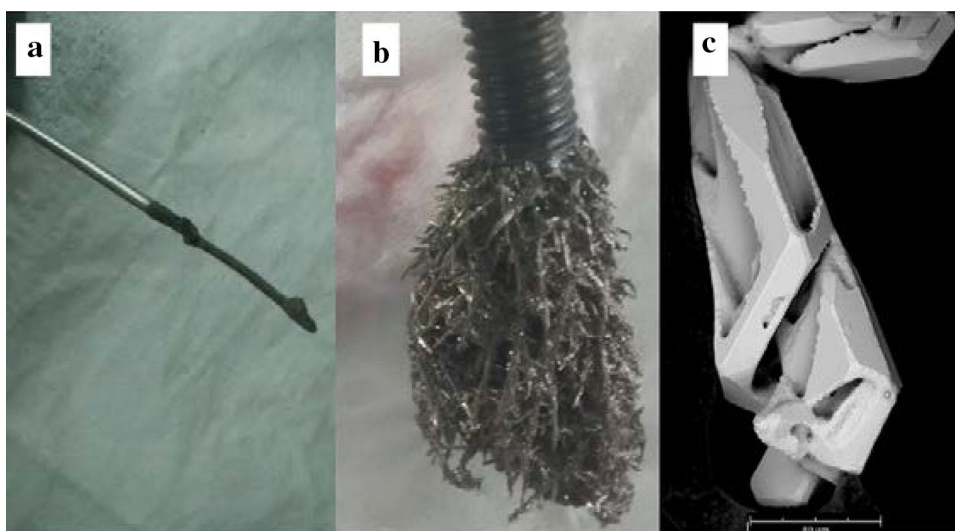
Fig. 3 Chronoamperogram during electrorefining under constant potential (-0.2 V) at 723 K in LiCl-KCl-NiCl_2 (0.58 wt%) melt. Working electrode: stainless steel screw (M6, active electrode area 7.22 cm^2)

possible to obtain high-purity Ni from a mixture of the two metals in molten salt if a suitable potential is applied. Since the Ni–Cr alloy dissolves in the melt during electrorefining, the deposition of metallic nickel occurs on the cathode while chromium remains in the electrolyte as Cr^{2+} which cannot be reduced at -0.2 V . Hence, we have used the constant potential technique during the electrorefining process.

To achieve further insight into the process of nickel deposition on the cathode during electrorefining, the chronoamperogram was recorded as shown in Fig. 3. The current associated with nickel deposition starts at -200 mA and decreases sharply to -135 mA in 10 s, which we attribute to the slow formation of the first nickel nuclei on the steel cathode [35, 36]. In the next 3590 s, the reduction current rises from -135 to -630 mA as a result of the increase in active surface area of the working electrode as more nickel is electrochemically deposited on the substrate. The current remains at about -630 mA for 1 h until the end of the electrorefining process. The Ni–Cr alloy immersed in LiCl–KCl melt becomes thinner after electrorefining (Fig. 4a) with a mass loss of 0.61 g. On the cathode, the products of electrorefining are mixed with chloride salts that adhere to the electrode. After washing the chlorides with deionized water, dendritic deposits are obtained, as illustrated in Fig. 4b.

SEM image of the cathodic deposits shows the presence of rod-like structures with holes and chips (Fig. 4c). The microstructure of the deposits formed in molten salt is completely different from the island-like surface morphology with cracked patterns formed in aqueous solutions [37]. The rods are several millimeters long and $\sim 80 \mu\text{m}$ wide, and the total weight of the collected products is 0.46 g. Thus, we find that almost all the dissolved nickel can be recovered, in accordance with Eq. 2; using Eq. 3,

Fig. 4 Photographs of **a** anodic Ni–Cr alloy after electrorefining; **b** deposits on the cathode; **c** SEM image of the deposits (color online)



the current efficiency can be calculated to be 71.27%. According to the cathodic reaction sequence, Cr³⁺ should be reduced to Cr²⁺ prior to the reduction of Ni²⁺ to Ni⁰ at – 0.2 V, which means that a fraction of the current passing through the cathode is consumed by the Cr³⁺ → Cr²⁺ reaction. This is similar to the process by which plutonium is separated from lanthanum by electrolysis in molten LiCl–KCl salt [38]. If it were not for the Cr³⁺ → Cr²⁺ reaction, the current efficiency of Ni electrorefining from Ni–Cr alloy would be 95.58%. As shown in Table 1,

$$R = m_{Ni}^{deposit} / m_{Ni}^{alloy}, \tag{2}$$

$$\eta = m_{Ni}^{deposit} / m_{Ni}^{theory}, \tag{3}$$

where $m_{Ni}^{deposit}$ and m_{Ni}^{alloy} are the masses of nickel in the deposit and in the alloy and m_{Ni}^{theory} is the calculated mass of nickel corresponding to the current passing through anode.

XRF, XRD, and ICP-AES measurements were carried out to determine the composition and purity of the deposits. In the XRF spectrum of the Ni–Cr alloy, peaks due to Ni and Cr are observed at 5.988 and 8.331 keV (Fig. 5). The first peak disappears in the spectrum of deposited products, suggesting that Ni is deposited on the cathode, whereas chromium remains dissolved in the molten salt. In addition,

the formation of metallic nickel on the cathode is confirmed from XRD results where only reflections originating from metallic Ni are observed (Fig. 6). The purity of nickel

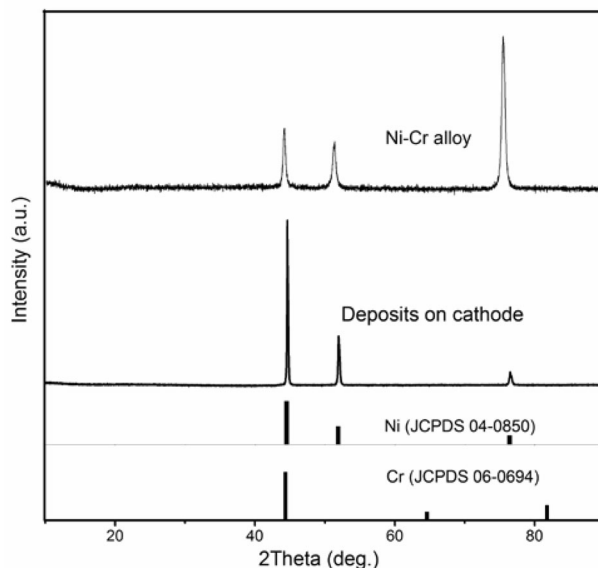


Fig. 6 XRD spectra of the Ni–Cr alloy and deposits on the cathode

Table 1 Impurity content in the Ni/Cr alloy before and after electrorefining

Contents (ppm)	Cr	Si	Sb	Mn	Al	Fe	Ti	Mo
Ni–Cr alloy	218,400	14,469	5051	3315	3034	2423	1800	1254
Product	102	3	ND	3	1	43	8	48

Fig. 5 XRF spectra of the Ni–Cr alloy and deposits on the cathode

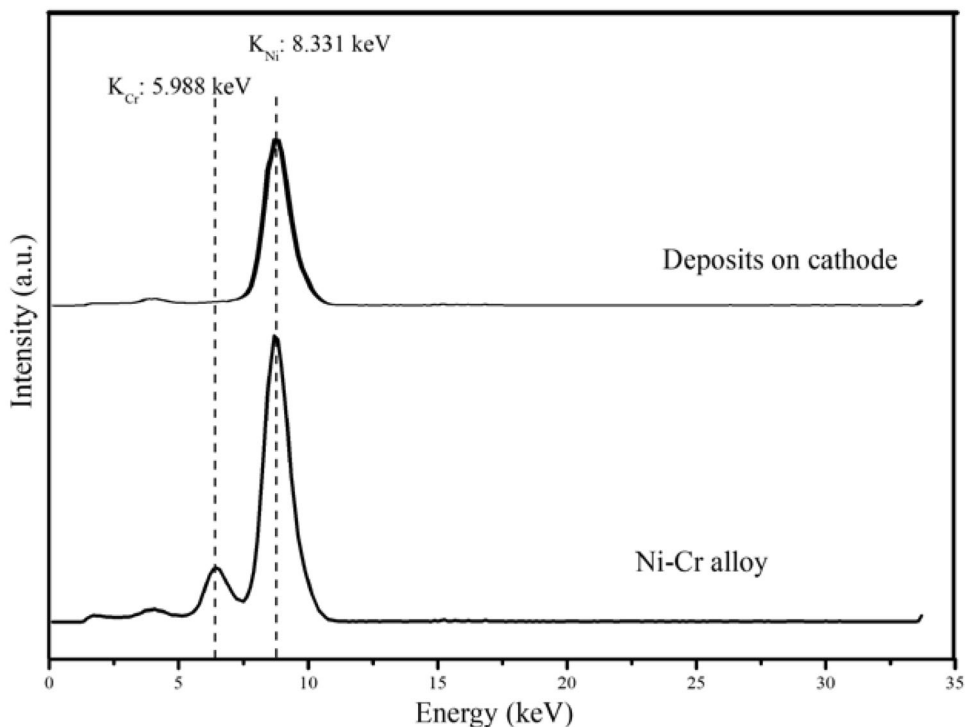
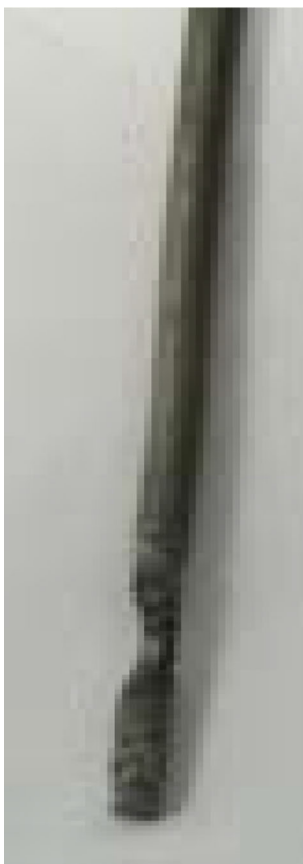


Table 2 Nickel recovery rate and current efficiency at different nickel concentrations

C_{NiCl_2} (wt%)	Mass loss of Ni– Cr alloy (g)	Amount of Ni in alloy (g)	Total charge (C)	Theoretical charge in Ni reduction (C)	Weight. of deposit on cathode (g)	Recovery rate (%)	Current efficiency (%)
0.58	0.61	0.45	2111	1574	0.46	102.22	95.58
1.15	0.34	0.25	1189	1052	0.29	116.00	90.16
2.23	0.50	0.36	1658	1461	0.43	120.34	95.37

**Fig. 7** Photograph of the anodic nickel rod after electrorefining at high NiCl_2 concentration (2.23 wt%)

in the deposits was determined to be higher than 99.83% by ICP-AES; the amounts of the other detected impurities are listed in Table 1. It is clear that the Cr content in the deposits decreases by three orders of magnitude compared to that in the starting Ni–Cr alloy and the impurity content in the deposits is significantly reduced upon electrorefining; thus, our results are better than those reported for Ni electrorefining CaCl_2 solution [39].

3.3 Influence of the nickel ion concentration in LiCl–KCl on electrorefining

The concentration of metal ions in the electrolyte has a significant influence on several aspects of the electrorefining process, such as deposition rate and product size

[40, 41]. According to our experimental results, at the same potential, the deposition rate of nickel increases as the concentration of nickel ions is raised (Table 2). At high nickel concentration, Ni^{2+} ions are rapidly reduced on the cathode, during which gaseous Cl_2 is formed simultaneously on the anode; similar phenomena have been observed in other molten salt systems [42]. Chlorine gas bubbles formed on the surface of the nickel anode can accumulate at gas–liquid interface [43], and the middle part of the nickel anode at the interface is corroded (Fig. 7) due to the formation of soluble NiCl_2 by the reaction of nickel with Cl_2 . Therefore, at high nickel concentrations, it is possible for the anodic nickel rod to fall into the electrolyte during electrorefining due to corrosion of the electrode, which obviously hinders the whole electrorefining process. At the low concentration (that was employed in our experiment), the nickel anode dissolves gradually from the bottom to the top and no obvious corrosion is observed (Fig. 4a). Our results thus reveal that a relatively low concentration of NiCl_2 in the molten electrolyte is favorable for the optimized deposition of Ni in the electrorefining process.

4 Conclusion

In this study, we have investigated the electrochemical behavior of Ni^{2+} and electrorefining of nickel from a nickel–chromium alloy in molten LiCl–KCl. Based on cyclic voltammetry and square wave voltammetry measurements, it was concluded that Ni^{2+} is directly reduced to Ni metal in LiCl–KCl and two electrons are exchanged in this process. Electrorefining of nickel under constant potential resulted in the formation of dendritic deposits on the stainless steel cathode. XRD and XRF of the deposits confirmed that these are composed only of nickel and no chromium was detected by ICP-AES analysis, indicating that the nickel content increased from 72.62 wt% in the alloy to 99.83 wt% in the deposits; nearly all the nickel (> 90%) could be recovered with high current efficiency. In addition, the electrorefining process was found to be significantly affected by the concentration of NiCl_2 in LiCl–KCl and decomposition of NiCl_2 occurred at high concentration, during which the generated chlorine gas accumulated around and reacted with the nickel anode at

the gas–liquid interface. Under these conditions, with continued electrorefining, due to the corrosion of the electrode, the anodic nickel rod could eventually fall into the electrolyte, implying that a low NiCl₂ concentration is favorable for nickel electrorefining. As an alternative to electrorefining in aqueous solutions, our experimental study offers a new route for the electrochemical purification of nickel in molten salt, in which both hydrogen evolution and gel formation due to the increase in pH can be avoided.

References

1. J. Montgomery, G.J. Sormunen, Nickel-catalyzed reductive couplings of aldehydes and alkynes. *Top. Curr. Chem.* **279**, 1–23 (2007). https://doi.org/10.1007/128_2007_139
2. M.D. Souza, L. Clave, V. Dubois, C.A.C. Perez, M. Schmal, Activation of supported nickel catalysts for carbon dioxide reforming of methane. *Appl. Catal. A Gen.* **272**(1–2), 133–139 (2004). <https://doi.org/10.1016/j.apcata.2004.05.026>
3. X.W. Chu, H.W. Cheng, C.T. Fu et al., Effect of thermal exposure time on tellurium-induced embrittlement of Ni–16Mo–7Cr–4Fe alloy. *Nucl. Sci. Tech.* **28**(12), 178 (2017). <https://doi.org/10.1007/s41365-017-0330-8>
4. J.H. Zhou, J.L. Tan, B. Sun et al., The protective performance of a molten salt frozen wall in the process of fluoride volatility of uranium. *Nucl. Sci. Tech.* **30**, 102 (2019). <https://doi.org/10.1007/s41365-019-0620-4>
5. L. Mond, C. Langer, F. Quincke, Action of carbon-monoxide on nickel (reprinted from *J Chem Soc*, vol 57, pp 749–753, 1890). *J. Organomet. Chem.* **383**(1–3), 1–5 (1990). [https://doi.org/10.1016/0022-328x\(90\)85117-h](https://doi.org/10.1016/0022-328x(90)85117-h)
6. H. Li, X. Liu, Y. Ma, B. Lai, Development status of carbonyl nickel production technology. *Powder Metall. Technol.* **29**(4), 290–295 (2011)
7. C.M. Whittington, K.L.K. Yeung, W.Y. Lo, Refined nickel anodes: pointers to industrial best practice. *Trans. Inst. Met. Finish.* **89**(3), 122–131 (2011). <https://doi.org/10.1179/174591911x13021847705806>
8. L. Wang, D. Liu, B. Yang et al., Purification of crude nickel by vacuum distillation. *J. Vac. Sci. Technol.* **30**(3), 283–287 (2010)
9. A. Aji, S. Purwadaria, J. Aromaa et al., The effect of gold on anode passivation and high current density operation under simulated silver electrorefining conditions. *Hydrometallurgy* **166**, 57–61 (2016). <https://doi.org/10.1016/j.hydromet.2016.09.004>
10. B. Jin, D.B. Dreisinger, A green electrorefining process for production of pure lead from methanesulfonic acid medium. *Sep. Purif. Technol.* **170**, 199–207 (2016). <https://doi.org/10.1016/j.seppur.2016.06.050>
11. R.R. Moskalyk, A.M. Alfantazi, Nickel sulphide smelting and electrorefining practice: a review. *Miner. Process. Extr. Metall. Rev.* **23**(3–4), 141–180 (2010). <https://doi.org/10.1080/08827500306893>
12. R. Wu, M. Oliyazadeh, A.M. Alfantazi, Electrical conductivity and density of NiSO₄/H₂SO₄ solutions in the range of modern nickel electrorefining and electrowinning electrolytes. *J. Appl. Electrochem.* **33**(11), 1043–1047 (2003). <https://doi.org/10.1023/a:1026261526134>
13. H.H. Abdel-Rahman, A.A. Harfoush, A.H.E. Moustafa, Effect of new diamine additives on rate and qualities of nickel deposition. *Trans. Inst. Met. Finish.* **91**(1), 32–43 (2013). <https://doi.org/10.1179/0020296712z.00000000061>
14. M.S. Moats, J.B. Hiskey, D.W. Collins, The effect of copper, acid, and temperature on the diffusion coefficient of cupric ions in simulated electrorefining electrolytes. *Hydrometallurgy* **56**(3), 255–268 (2000). [https://doi.org/10.1016/s0304-386x\(00\)00070-0](https://doi.org/10.1016/s0304-386x(00)00070-0)
15. J. Peng, X.B. Zheng, Y.X. Liu et al., Influence of α -Al₂O₃ and AlF₃ on pyrohydrolysis of Li₃AlF₆. *Nucl. Sci. Tech.* **29**, 125 (2018). <https://doi.org/10.1007/s41365-018-0465-2>
16. W.T. Zhou, J.S. Zhang, Chemical diffusion coefficient calculation of U³⁺ in LiCl–KCl molten salt. *Prog. Nucl. Energy* **91**, 170–174 (2016). <https://doi.org/10.1016/j.pnucene.2016.04.017>
17. G.M. Haarberg, T. Store, R. Tunold, Metal deposition from chloride melts: I. Rates of diffusion in solvent melt. *Electrochim. Acta* **76**, 256–261 (2012). <https://doi.org/10.1016/j.electacta.2012.05.003>
18. C.H. Lee, D.Y. Kang, M.K. Jeon et al., Addition effect of fluoride compounds for Zr electrorefining in LiCl–KCl molten salts. *Int. J. Electrochem. Sci.* **11**(1), 566–576 (2016)
19. T. Takenaka, S. Isazawa, M. Mishina et al., Electrorefining of magnesium in molten salt and its application for recycling. *Mater. Trans.* **44**(4), 546–551 (2003). <https://doi.org/10.2320/matertrans.44.546>
20. Y.H. Kang, S.C. Hwang, H.S. Lee et al., Effects of neodymium oxide on an electrorefining process of uranium. *J. Mater. Process. Technol.* **209**(11), 5008–5013 (2009). <https://doi.org/10.1016/j.jmatprotec.2009.01.024>
21. V. Schwarz, H. Wendt, Electrorefining of aluminum scrap from chloride melts. *J. Appl. Electrochem.* **25**(1), 34–40 (1995)
22. J. Cai, X.T. Luo, G.M. Haarberg et al., Electrorefining of metallurgical grade silicon in molten CaCl₂ based salts. *J. Electrochem. Soc.* **159**(3), D155–D158 (2012). <https://doi.org/10.1149/2.041203jes>
23. T. Zhu, W. Huang, H. Zheng et al., Investigating the influence of F[−] on U⁴⁺ in molten LiCl–KCl–UF₄ system and electro-deposition of U. *J. Radioanal. Nucl. Chem.* **312**(3), 479–485 (2017). <https://doi.org/10.1007/s10967-017-5242-x>
24. X.B. Wang, W. Huang, Y. Gong et al., Electrochemical behavior of Th(IV) and its electrodeposition from ThF₄–LiCl–KCl melt. *Electrochim. Acta* **196**, 286–293 (2016). <https://doi.org/10.1016/j.electacta.2016.02.184>
25. W. Huang, L. Tian, C. She et al., Electrochemical behavior of europium(III)–europium(II) in LiF–NaF–KF molten salt. *Electrochim. Acta* **147**, 114–120 (2014). <https://doi.org/10.1016/j.electacta.2014.08.119>
26. F. Jiang, W. Huang, H. Zheng et al., Electrochemical behavior and electrowinning of uranium(IV) from FLiNaK molten salt. *J. Radioanal. Nucl. Chem.* **311**(3), 1891–1897 (2017). <https://doi.org/10.1007/s10967-016-5160-3>
27. L. Massot, A.L. Bieber, M. Gibilaro et al., Silicon recovery from silicon–iron alloys by electrorefining in molten fluorides. *Electrochim. Acta* **96**, 97–102 (2013). <https://doi.org/10.1016/j.electacta.2013.02.065>
28. A.L. Bieber, L. Massot, M. Gibilaro et al., Silicon electrodeposition in molten fluorides. *Electrochim. Acta* **62**, 282–289 (2012). <https://doi.org/10.1016/j.electacta.2011.12.039>
29. A. Cotarta, J. Bouteillon, J.C. Poignet, Electrochemistry of molten LiCl–KCl–CrCl₃ and LiCl–KCl–CrCl₂ mixtures. *J. Appl. Electrochem.* **27**(6), 651–658 (1997). <https://doi.org/10.1023/a:1018475401848>
30. L.L. Su, K. Liu, Y.L. Liu et al., Electrochemical behaviors of Dy(III) and its co-reduction with Al(III) in molten LiCl–KCl salts. *Electrochim. Acta* **147**, 87–95 (2014). <https://doi.org/10.1016/j.electacta.2014.09.095>
31. Y.V. Pleskov, A.J. Bard, L.R. Faulkner, *Electrochemical methods: fundamentals and applications*, New York: Wiley, 2001, 2nd

- ed. Russ. J. Electrochem. **38**(12), 1364–1365 (2002). <https://doi.org/10.1023/a:1021637209564>
32. Y.L. Liu, G.A. Ye, L.Y. Yuan et al., Electroseparation of thorium from ThO_2 and La_2O_3 by forming Th–Al alloys in LiCl–KCl eutectic. *Electrochim. Acta* **158**, 277–286 (2015). <https://doi.org/10.1016/j.electacta.2015.01.128>
33. Y.L. Liu, Y.D. Yan, W. Han et al., Electrochemical separation of Th from ThO_2 and Eu_2O_3 assisted by AlCl_3 in molten LiCl–KCl. *Electrochim. Acta* **114**, 180–188 (2013). <https://doi.org/10.1016/j.electacta.2013.09.154>
34. Y. Liu, K. Liu, L. Luo et al., Direct separation of uranium from lanthanides (La, Nd, Ce, Sm) in oxide mixture in LiCl–KCl eutectic melt. *Electrochim. Acta* **275**, 100–109 (2018). <https://doi.org/10.1016/j.electacta.2018.04.140>
35. M.R. Bermejo, J. Gomez, J. Medina et al., The electrochemistry of gadolinium in the eutectic LiCl–KCl on W and Al electrodes. *J. Electroanal. Chem.* **588**(2), 253–266 (2006). <https://doi.org/10.1016/j.jelechem.2005.12.031>
36. Y. Castrillejo, M.R. Bermejo, A.I. Barrado et al., Electrochemical behaviour of dysprosium in the eutectic LiCl–KCl at W and Al electrodes. *Electrochim. Acta* **50**(10), 2047–2057 (2005). <https://doi.org/10.1016/j.electacta.2004.09.013>
37. P. Souček, F. Lisý, R. Tuláček et al., Development of electrochemical separation methods in molten LiF–NaF–KF for the molten salt reactor fuel cycle. *J. Nucl. Sci. Technol.* **42**(12), 1017–1024 (2005). <https://doi.org/10.1080/18811248.2005.9711054>
38. J. Serp, P. Lefebvre, R. Malmbeck et al., Separation of plutonium from lanthanum by electrolysis in LiCl–KCl onto molten bismuth electrode. *J. Nucl. Mater.* **340**(2–3), 266–270 (2005). <https://doi.org/10.1016/j.jnucmat.2004.12.004>
39. J.L. Sabot, R. Rosset, Electrorefining of ferronickels. *Electrochim. Acta* **21**(11), 925–934 (1976). [https://doi.org/10.1016/0013-4686\(76\)85067-0](https://doi.org/10.1016/0013-4686(76)85067-0)
40. J. Yu, K.Y. Cha, D.J. Seo et al., Effect of the concentration of cobalt chloride solution for the preparation of nano-sized cobalt oxide powder by spray pyrolysis process. *Korean J. Mater. Res.* **24**(6), 277–284 (2014)
41. Y.K. Kim, Effect of salt on crystal growth of plate-like alumina particles by molten-salt method. *Korean J. Chem. Eng.* **53**(5), 603–608 (2015)
42. P. Souček, R. Malmbeck, E. Mendes et al., Exhaustive electrolysis for recovery of actinides from molten LiCl–KCl using solid aluminium cathodes. *J. Radioanal. Nucl. Chem.* **286**(3), 823–828 (2010). <https://doi.org/10.1007/s10967-010-0739-6>
43. F. Lantelme, H. Alexopoulos, O. Haas, Role of gas-bubbles adsorbed on a carbon electrode: electroreduction of chlorine gas in fused-salts. *J. Appl. Electrochem.* **19**(5), 649–656 (1989). <https://doi.org/10.1007/bf01320639>